Earth and Planetary Science Letters 307 (2011) 59–70

Contents lists available at ScienceDirect

Earth and Planetary Science Letters

journal homepage: www.elsevier.com/locate/epsl

Heat production and geotherms for the continental lithosphere

D. Hasterok *, D.S. Chapman

Department of Geology & Geophysics, University of Utah, Salt Lake City, UT, USA

ARTICLE INFO

Article history:
Received 26 July 2010
Received in revised form 14 April 2011
Accepted 18 April 2011
Available online 17 May 2011

Editor: Y. Ricard

Keywords:
continental lithosphere
heat generation
geotherm
xenolith thermobarometry
craton

ABSTRACT

We propose a continental lithosphere heat production model based on the petrology of crust and mantle, heat production measurements of surface and xenolith samples, and tectono-thermal constraints. Continental elevation considered within a thermal isostasy rubric is used to partition crustal heat production into upper crustal and lower crustal contributions. The best-fitting partition model using elevation data from 33 North American tectonic provinces suggests upper crustal heat production on average accounts for ~6% of observed surface heat flow. An average heat production for the lower crust of 0.4 $\mu W/m^3$ is based on measurements from exposed granulite terranes while a lithospheric mantle heat production of 0.02 $\mu W/m^3$ is based on chemical analyses of mantle xenoliths. Results are relatively insensitive to mantle composition and thickness of the upper crustal heat producing layer. Continental geotherms are computed using the generalized heat production model and incorporating thermal conductivity results from a number of recent laboratory studies. *P–T* conditions of xenoliths provide further constraints to ensure that our geotherms and hence the heat production model are reasonable. *P–T* conditions of 10 Precambrian regions are consistent with surface heat flow of 40 mW/m^2 and a lithospheric thickness of 200 km. Our generalized model for heat production can serve as a reference model from which anomalies are identified.

1. Introduction

Radiogenic heat generation (HG) within the lithosphere, created by the decay of K, Th, and U, accounts for an estimated 30–40% of heat loss through the continents (Artemieva and Mooney, 2001; Hasterok and Chapman, 2007b; Pollack and Chapman, 1977; Vitorello and Pollack, 1980). Accurate estimates of HG are necessary for computing lithospheric temperatures and heat flow (HF) across both the Moho and the lithosphere–asthenosphere boundary, as well as many physical parameters that depend upon temperature (e.g., density, seismic velocity, viscosity, elevation) all of which have important geodynamic implications (e.g., Flowers et al., 2004; Hyndman et al., 2005; Jaupart and Mareschal, 1999; Sandiford and McLaren, 2002). However, reliable estimates of HG are difficult to obtain at depths greater than a few hundred meters using common geophysical and geochemical exploration methods, making it one of the least constrained physical parameters within the lithosphere. Therefore, it is desirable to have a general HG model that can be used as both a reference for comparison, and a starting model for thermal and geodynamic studies of the lithosphere.

Several general models for HG exist, but they are based on crustal age (Jaupart and Mareschal, 2003), which poorly correlates with HG, or are calibrated only for shield and cratonic regions (Rudnick and Nyblade, 1999; Rudnick et al., 1998). Neither of these model types adequately reflects the chemical differentiation of the crust, therefore, leading to an over-prediction of temperatures (Jaupart and Mareschal, 2007). Models based on HG–HF relationships derived from a collection of geologic/tectonic provinces show promise because they implicitly assume both a decrease in HG with increasing juvenile crustal age and an increase in mantle HF in active tectonic regions (Artemieva and Mooney, 2001; Chapman, 1986). These partition models are generally applied as a function of a single observable, surface HF.

Recent analyses of lithospheric HG (Artemieva and Mooney, 2001; Jaupart and Mareschal, 2003, 2007) focus on surface HG measurements and a heat budget approach as primary constraints. This paper builds on these previous analyses by exploring two additional constraints. First, we note that temperature–depth profiles are extremely sensitive to HG distributions and use continental elevation as a measure of the average temperature of the entire lithosphere (Hasterok and Chapman, 2007a,b). Here we are following the lesson of using oceanic bathymetry in successfully constraining models for the thermal evolution of oceanic lithosphere. Specifically, we exploit a set of compositionally normalized elevation data to partition lithospheric HG into upper crustal enhanced HG and contributions from the lower crust and mantle lithosphere. Second, we require geotherms computed from a preferred HG model to pass through temperature–depth space occupied by *P–T* conditions inferred for mantle xenoliths.

A generalized HG model for the lithosphere is not intended to characterize all geographic regions of the continents. There is a

* Corresponding author at: IGPP, Scripps Institution of Oceanography, La Jolla, CA, USA.
E-mail addresses: dhasterok@gmail.com (D. Hasterok), David.Chapman@utah.edu (D.S. Chapman).

0012-821X/$ – see front matter © 2011 Elsevier B.V. All rights reserved.
doi:10.1016/j.epsl.2011.04.034

parallel here to the use of the Preliminary Reference Earth Model (PREM) (Dziewonski and Anderson, 1981) in seismology. PREM represents the global average seismic velocity and density versus depth; it does not necessarily exist anywhere on Earth, but represents a convenient reference from which seismic anomalies may be identified. Our reference model differs from PREM since it applies only to continents rather than globally and is laterally parameterized in one value (surface HF) as opposed to constant. The reference HG model and analysis in this paper provide both a model and a means of identifying HG anomalies and their consequences for the thermal state of the lithosphere.

2. Geotherm sensitivity to heat production

Lithospheric temperatures and thickness are sensitive to the magnitude and vertical distribution of HG. The effect of HG variations on the geotherm is illustrated by perturbing a simple three-layered model (Fig. 1). Consider a lithosphere, with a high upper crustal HG (1 $\mu W/m^3$), a depleted lower crust (0.4 $\mu W/m^3$), and a low mantle HG (0.02 $\mu W/m^3$). For this test, we define a reference geotherm with an intermediate surface HF of 60 mW/m^2 (see Section 5.1 for geotherm construction). This reference geotherm reaches the 1300 °C adiabat at ~90 km, assumed to identify the lithosphere–asthenosphere boundary. By varying only the HG within each layer individually by ± 25 and $\pm 50\%$ we investigate the sensitivity of temperatures and lithospheric thickness to the depth of the HG anomaly.

A $\pm 50\%$ variation in upper crustal HG produces a difference in lithospheric thickness of ~50 km and >400 K temperature variation at 75 km. The effect of ± 25 and $\pm 50\%$ lower crustal HG variance results in 10 km and 20 km lithospheric thickness estimates, respectively. The temperature difference is significantly smaller (~175 K at 75 km for $\pm 50\%$ variation) than differences resulting from similar percentage variations in the upper crustal HG. Mantle HG variations have little effect on lithospheric temperature. In order to rival the lithospheric thickness variation seen in the lower crustal case, mantle HG would have to vary by greater than $\pm 400\%$.

These simple tests demonstrate that deviations from average lower crustal and lithospheric mantle HG can be easily masked by upper crustal uncertainties. Therefore, we focus our analysis on variations in upper crustal HG.

3. Previous models

Several models for crustal and/or lithospheric HG exist, each using different constraints. Allis (1979) and Rybach and Buntebarth (1984) suggested using seismic velocities to predict HG, but HG for any given rock is highly non-unique. Attempts to estimate crustal HG using xenolith *P–T* conditions provide reasonable averages (0.5–0.8 $\mu W/m^3$) (Rudnick et al., 1998), but are only calibrated to Precambrian provinces. Rudnick and Nyblade (1999) used xenolith *P–T* conditions to test mantle as well as crustal HG. Best-fitting values for two parameters, crustal HG and crustal thickness, fall within the tested bounds, but the remaining three grid search parameters lie on the boundary of the restricted test range, including mantle HG, crustal conductivity, and surface HF. The large number of parameters falling on the boundary of the input range suggests that the model space is too restrictive or some of the physics necessary to describe the thermal state accurately is not included (e.g., *P–T* dependent thermal conductivity).

Jaupart and Mareschal (2003) use surface HF constraints to make an elegant estimate of crustal HG and find a significant variation in crustal HG with juvenile crustal age. They suggest the present-day bulk-crustal HG increases from ~0.65 $\mu W/m^3$ in Archean to ~0.87 $\mu W/m^3$ in Phanerozoic terranes. However, the correlation between age and HG is weak (Rao et al., 1982). For example, the Wopmay orogen and much of Precambrian Australia have anomalously high HF due to high upper-crustal radioactivity (Lewis et al., 2003; McLaren et al., 2003). Additionally, a geotherm constructed using the HG models by Jaupart and Mareschal (2003) ignores the chemical stratification of the lithosphere, resulting in significantly higher temperature estimates throughout the lithosphere (Jaupart and Mareschal, 2007).

Artemieva and Mooney (2001) and Chapman (1986) take a different approach, estimating upper crustal HG from an empirically derived partitioning of surface HF between an enriched upper crustal radiogenic HF (q_{rad}) and reduced (or basal, q_b) HF (Pollack and Chapman, 1977). While many use the term basal HF to refer to the HF at the base of the lithosphere, we use the term to refer to HF at the base of the upper crustal radiogenically enriched layer as originally used by Pollack and Chapman (1977). Partition (q_b:q_{rad}) estimates range from 60:40 (Pollack and Chapman, 1977; Vitorello and Pollack, 1980) to 67–71:33–29 (Artemieva and Mooney, 2001). A major advantage of the partitioning model, compared with the other models discussed above, is a dependence on surface HF, an observable that directly responds to changes

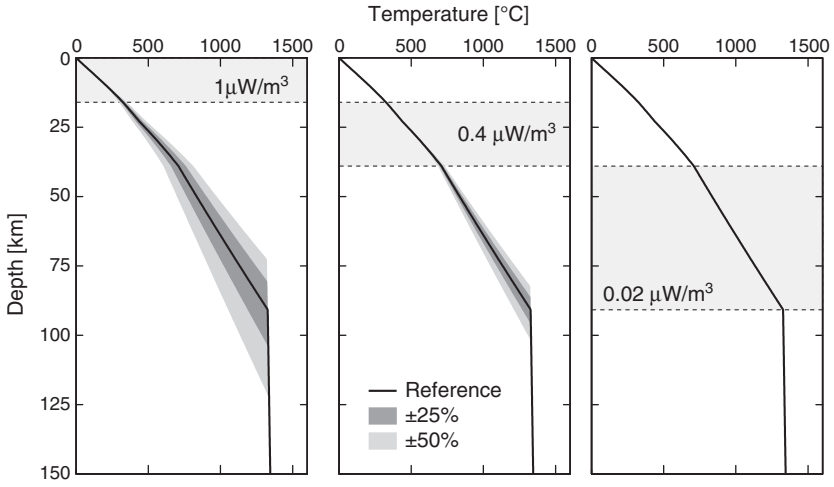

Fig. 1. Temperature sensitivity to 25 and 50% variations in heat production of the upper crust (left), lower crust (middle), and upper mantle (right). The reference geotherm is computed with heat production of 1 $\mu W/m^3$ upper crust, 0.4 $\mu W/m^3$ lower crust and 0.02 $\mu W/m^3$ for upper mantle. Geotherms are computed with a surface heat flow of 60 mW/m^2, upper crustal thickness of 16 km, and Moho depth of 39 km.

in upper crustal radioactivity. Thus the partition model can be applied generally to any region where surface HF is observed or can be estimated. Because of the intrinsic connection to surface HF, the partition model implicitly assumes that tectonically active regions frequently have higher than average mantle HF and a decrease in HG with age.

4. Measured heat production constraints

A general HG model for the continental lithosphere, requires the range of HG and the general variation with depth. Heat production observations and estimates are summarized below for each of the lithospheric layers.

4.1. Upper crust

Direct measurements of HG indicate generally high values in felsic rocks (~2 μW/m^3), low in mafic rocks (~0.2 μW/m^3) and very low in ultramafic rocks (~0.02 μW/m^3). Variations of HG within individual and well-sampled terranes can vary by at least an order of magnitude over small spatial scales (<1 km) (Kukkonen and Lahtinen, 2001; Ray et al., 2003). Individual terranes commonly have standard deviations 50–100% of the sample mean or greater, and frequently exhibit non-Gaussian distributions (e.g., Brady et al., 2006; Jaupart and Mareschal, 2003; Jõeleht and Kukkonen, 1998; Ketcham, 2006). Airborne radiometric surveys provide good spatial averages, but the depth of penetration is <30 cm and often does not see through sedimentary cover (Bodorkos et al., 2004). Few terranes, however, have been subjected to sufficiently detailed HG investigations necessary to provide robust estimates for modeling HF.

Even when good surface spatial averages can be obtained, HG variation with depth is still problematic. Three functional forms have been proposed (Lachenbruch, 1970; Roy et al., 1968): constant value layers, linearly decreasing, and exponentially decreasing. The exponential model was developed to explain observations of HF–HG patterns observed in granitic batholiths with differing levels of surface erosion (Lachenbruch, 1968, 1970; Swanberg, 1972).

Some constraints on vertical HG variation come from deep boreholes and exposed crustal cross-sections. The research wells KTB in Germany and Kola SG-3 in Russia are the deepest scientific boreholes at 9 and 12.2 km, respectively. KTB is drilled into a series of layered gneiss and metabasites and SG-3 is drilled into a Precambrian volcanic and metamorphic terrane. The HG for each well shows a reasonable correlation to rock type (Clauser et al., 1997; Popov et al., 1999) but an irregular pattern with depth. The Chinese scientific borehole (CCSD-MH) also exhibits a correlation to lithology (He et al., 2008); however, HG is quite variable within any given lithologic unit. Even within boreholes drilled predominantly into granite, HG can be highly variable (Balling et al., 1990; Lachenbruch and Bunker, 1971; Vigneresse and Cuney, 1991). No single functional form can explain the patterns of HG with depth for these boreholes.

Exposed crustal sections that can be related to pseudo-depth profiles provide greater spatial coverage, extending knowledge to greater depths than boreholes. Measurements of HG have been collected in metamorphic core complexes (Catalina and Harquahala Mountains (Ketcham, 2006)), impact structures (Vredefort and Sudbury (Nicolaysen et al., 1981; Schneider et al., 1987)), thrust sheets (Zentralgneis, Wawa-Foleyet, Pikwitonei-Sachigo, Hidaka Arc, and Arunta-Musgrave (Ashwal et al., 1987; Fountain et al., 1987; Furukawa and Shinjoe, 1997; Hawkesworth, 1974; McLaren et al., 2003)), structural folds (Egersund-Bamble, Erzgebirge (Förster and Förster, 2000; Pinet and Jaupart, 1987)), and batholiths (Idaho Batholith, Sierra Nevada Mountains, and Closepet Granite batholith (Brady et al., 2006; Roy et al., 2008; Swanberg, 1972)). These exposed sections also show little correlation of HG with estimated depth beyond a general pattern of higher values near the surface where felsic rocks are dominant and lower values in mafic rocks of the lower crust. In regions where thrust sheets duplicate parts of the crustal section, HG often exhibits a repeating pattern (Clauser et al., 1997; He et al., 2008; Ketcham, 2006; McLaren et al., 2003).

Given the poor correlation of HG with depth in the upper crust, we suggest a reference model with a constant upper crustal HG. A constant HG with depth is also the least complicated functional form, making it easy to compute relative anomalies.

4.2. Lower crust

Studies of seismic velocity and equilibrium conditions from xenoliths suggest that the lower crust is more mafic on average than the upper crust and best described by granulite metamorphic facies (Christensen and Mooney, 1995; Rudnick and Fountain, 1995). Observations from exposed granulite terranes and xenoliths provide the best insight for estimating lower crustal HG (Rudnick and Fountain, 1995). Geochemical abundances of heat producing elements (HPE's) are converted to HG, A, by

$$A = 10^{-5}\rho\left[3.5C_{K_2O} + 9.67C_U + 2.63C_{Th}\right], \quad (1)$$

with concentrations of K_2O in wt.%, and of U and Th in ppm. We assume densities, ρ, of 2800, 2850, and 3000 kg/m^3 for felsic, intermediate, and mafic granulites, respectively.

Heat production measurements from 31 exposed granulite terranes range from 0.1 to 2.7 μW/m^3 with a mean of 0.68±0.62 μW/m^3 and a median 0.45 μW/m^3 (Fig. 2). In general, the higher HG terranes are felsic rather than mafic granulites. If only mafic granulites are considered, the mean HG is 0.36±0.50 μW/m^3 with a median of 0.15 μW/m^3. However, it is difficult to derive completely independent estimates of mafic and felsic granulites using this dataset because the reported HG values are commonly terrane averages rather than separated into mafic and felsic compositions. Lower crustal xenolith-derived HG values are lower on average than from exposed terranes with means (medians) of felsic, intermediate, and mafic granulites of 0.85 (0.57), 0.20 (0.09), and 0.13 (0.06) μW/m^3, respectively (Rudnick and Fountain, 1995). This difference could be due to metasomatic processes that affect surface exposures or xenoliths during exhumation and/or near surface groundwater flow (Jaupart and Mareschal, 2003).

We assume the middle crustal HG is the same as in the lower crust because the temperature sensitivity to middle and lower crustal HG variations is small relative to the upper crust. The mid-crustal layer is not pervasive globally (Rudnick and Gao, 2003), and where it exists, tends to have HG more similar to lower rather than to upper crust. Our model includes a value of 0.4 μW/m^3 for the lower crust, which is slightly higher than typical for mafic granulite and lower than most intermediate compositions such as amphibolite and tonalite.

4.3. Lithospheric mantle

Xenoliths provide the best estimates of mantle HG on continents. Average HG from compilations of continental lithospheric peridotites varies from 0.006 μW/m^3 in exposed off-craton massifs to 0.044 μW/m^3 in cratonic xenoliths (Rudnick et al., 1998). However, xenoliths, particularly kimberlites, are subject to significant disturbances by metasomatic processes during ascent. Excluding kimberlite xenoliths, the median HG for cratonic peridotites is estimated to be 0.019 μW/m^3 (Rudnick et al., 1998). In general, bulk U and Th concentrations are rarely measured in xenoliths. The above HG estimates are based on assumed abundances of U and Th relative to K concentration (Rudnick et al., 1998).

The HPE's U and Th are typically found in monazite, a phosphate mineral similar to apatite. Studies focusing on apatite in mantle peridotites suggest that even at very small concentrations, apatite can dominate HG (Ionov et al., 1996; O'Reilly and Griffin, 2000; O'Reilly et al., 1997). For example, 1% by weight apatite in a mantle rock can

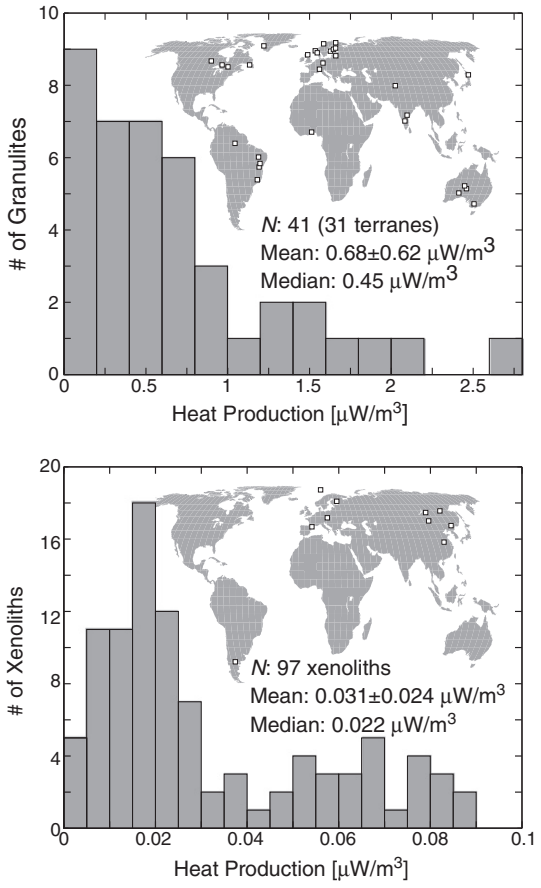

Fig. 2. Heat production from granulite terranes (top) and mantle xenoliths (bottom). Locations are shown on inset maps. Mean values are given ± one standard deviation. Granulite data from Ashwal et al. (1987), Attoh and Morgan (2004), Brady et al. (2006), Del Lama et al. (1998), Förster and Förster (2000), Fountain et al. (1987), Garrido et al. (2006), Hölttä (1997), Kukkonen and Jõeleht (1996), Martignole and Martelat (2005), Owen et al. (2003), Pinet and Jaupart (1987), Ray et al. (2003) and references therein. Xenolith data from Ackerman et al. (2007), Bianchini et al. (2007), Bjerg et al. (2005), Ionov (2004), Ionov et al. (1993, 2002, 2005) Peltonen et al. (1999), Rudnick et al. (2004), Wiechert et al. (1997), and Xu et al. (1998).

increase the total HG by 0.3 μW/m^3. Since apatite is a common accessory mineral but rarely reported, it is unknown whether these high HG values are widespread or isolated locally (Ionov et al., 1996; O'Reilly and Griffin, 2000; O'Reilly et al., 1997). However, the minor to negligible curvature in xenolith *P–T* estimates suggests mantle HG is on average very small.

We compiled HG for several xenolith localities that include K_2O, U, and Th in the bulk chemical analysis (Fig. 2). Heat production is computed using Eq. (1) with an assumed density of 3300 kg/m^3. Total HG for these xenoliths ranges from 0.003 to values greater than 1 μW/m^3 with two exceptionally high values $\gg 1$ μW/m^3. In general, the values >0.1 μW/m^3 come from localities showing signs of metasomatism (e.g., Jericho xenoliths on the Slave craton from Russell et al. (2001)). A strong peak in the estimated mantle HG histogram occurs below ~0.02 μW/m^3. When restricted to values less than 0.1 μW/m^3, average HG is 0.031 ± 0.024 μW/m^3 and a median of 0.022 μW/m^3. In our models, we assume a HG of 0.02 μW/m^3 for the mantle lithosphere.

5. Methods

5.1. Geotherms

One-dimensional steady-state conductive geotherms are computed using a boot-strapping method (Chapman, 1986), which requires thermal conductivity, HG, surface temperature, and surface HG as inputs. The vertical column is divided into arbitrarily thin layers, for which properties can be considered constant. Temperature, T_{i+1}, and HF, q_{i+1}, at the bottom of each layer are determined from the temperature, T_i, and HF, q_i, at the top of each layer by

$$T_{i+1} = T_i + \frac{q_i}{\lambda_i}\Delta z_i - \frac{A_i}{2\lambda_i}\Delta z_i^2, \tag{2}$$

and

$$q_{i+1} = q_i - A_i \Delta z_i, \tag{3}$$

where A_i and λ_i are the intra-layer HG and conductivity, respectively. The layer thickness is given by Δz_i and set to 100 m. Because we use a *P–T*-composition dependent thermal conductivity model, a Newton–Raphson iterative scheme is employed to solve for temperature T_{i+1} and the intra-layer conductivity. Pressure is computed using a logarithmic equation of state (Poirier and Tarantola, 1998).

We estimate thermal conductivity from an assumed mineralogic composition of the lithosphere determined by average oxide compositions and common rock types. The assumed compositional model is equivalent to a granodiorite upper crust (0–16 km), tonalite middle crust (16–23 km), and mafic granulite for the lower crust (23–39 km) (Table 1). Layer thicknesses and composition for the crust roughly correspond to estimates discussed by Rudnick and Gao (2003). Because we use compositional layering as a constraint on thermal conductivity, conductivity can be discontinuous with depth resulting in slight kinks in the geotherms (Supplement Fig. S.2).

Average mantle compositions are based on garnet xenocryst estimates by (Griffin et al., 1999). Their peridotite compositions are derived from garnet xenocrysts and correspond approximately to average Archean, Proterozoic, and Phanerozoic continental lithospheric mantle. Garnet peridotites are converted to spinel-peridotites via 2 *orthopyroxene* + *spinel* ↔ *garnet* + *olivine*. The transition depth is estimated by the intersection of the geotherm and an empirically derived phase boundary,

$$P_{sg}(T) = 1.4209 + exp\left(3.9073 \times 10^{-3} T - 6.8041\right), \tag{4}$$

where T is absolute temperature in Kelvin. This curve is calibrated by inversion of the data reported by Klemme and O'Neill (2000),

Table 1
Compositional model used to compute geotherms.

Mineral	Crust[a]				Mantle[b]	
	Upper	Middle	Lower	Archon	Proton	Tecton
Quartz	27	15	2			
Orthoclase	15	5	10			
Albite	32	35	10			
Anorthite	8	20	18			
Phlogopite	5					
Hornblende	13	20	47			
Diopside			1	1.96	5.47	9.97
Hedenbergite			1	0.14	0.53	1.03
Enstatite		2	1	23.22	15.47	15.37
Ferrosillite		3	1	1.78	1.53	1.63
Forsterite				64.04	63.65	54.20
Fayalite				4.96	3.35	5.80
Pyrope				3.19	5.58	9.57
Almandine			9	0.81	1.42	2.43

[a] Upper crust composition is a granodiorite similar to St. Cloud Granodiorite described by Hanley et al. (1978). The mid-crustal composition is assumed to be similar to a tonalite–trondhjemite–granodiorite (TTG). Lower crustal composition is a mafic granulite similar to a sample by Ray et al. (2006). Crustal compositions roughly correspond to oxide averages given by Rudnick and Gao (2003).

[b] Mantle compositions are derived from garnet xenocrysts and approximate Archean (Archon), Proterozoic (Proton), and Phanerozoic (Tecton) mantle (Griffin et al., 1999).

Robinson and Wood (1998), Walter et al. (2002) and references therein.

5.1.1. Heat generation

Assuming steady-state conditions, surface HF results from a combination of HF into the base of the lithosphere and the integrated HG within the lithosphere. As discussed above, temperatures are very sensitive to variations in upper crustal HG (Fig. 1). Therefore, we focus only on variations in upper-crustal HG and fix all other layers at constant values. Thus the mid-crustal, lower crustal, mantle HG, and sub-lithospheric HF can be combined into a single parameter, basal HF (q_b). The surface HF, q_s, can then be written,

$$q_s = q_b + A_{\mathrm{UC}}D \tag{5}$$

where A_{UC} is the upper crustal HG, D is the thickness of the upper crustal HG layer, and the product $A_{\mathrm{UC}}D$ is the radiogenic HF in the upper crust.

We use Eq. (5) to define three classes of HG models. Class I — invariant upper crustal HG where HG is independent of the surface HF and all variations in surface HF result from differences in lithospheric thickness and variation in sub-lithospheric HF. Class II — constant basal HF, where all variations in surface HF result from changes in upper crustal HG. Hence the upper crustal HG can be computed by

$$A_{\mathrm{UC}} = (q_s - q_b)/D. \tag{6}$$

The invariant HG model would be most applicable in regions such as rifts where significant variations in basal HF occur, but the average crustal HG may be relatively constant (McKenzie, 1978). Models with constant basal HF may best describe individual shields and cratons where the basal HF is believed to be relatively constant and variations in surface HF are still observed (Jaupart and Mareschal, 2003). Globally, the patterns of surface HF are likely to result from a combination of these end-member models, hence the basal HF represents only a fraction of the total HF (i.e., $q_b = Fq_s$). Thus, Class III — the partition model can be written,

$$A_{\mathrm{UC}} = (1-F)q_s/D, \tag{7}$$

where F is the partition coefficient. This partition model has been used with success in describing global HF/HG patterns (Artemieva and Mooney, 2001; Pollack and Chapman, 1977; Vitorello and Pollack, 1980) and in developing a thermal isostatic relationship for North America (Hasterok and Chapman, 2007b).

Geotherms computed in this study are modeled using constant HG within the upper crustal HG layer rather than the commonly used exponential decreasing HG layer for two reasons. First, the commonly employed exponential decreasing HG models with depth can exceed 5 μW/m^3 for reasonable partition models with high HF. Regional surface HG values this high are rarely observed except in provinces that may be identified by their associated high HF and low adjusted elevation such as the Wopmay orogen, Lachen Fold Belt, and the North and South Australian cratons (Fig. 3; (Lewis et al., 2003; McLaren et al., 2003)). The second rationale for using constant HG stems from highly variable HG observations in exposed crustal sections and deep boreholes as discussed in Section 4.1.

Heat production in the middle to lower crust is assumed to be 0.4 μW/m^3, consistent with granulite terranes. Mantle HG is set to 0.02 μW/m^3 as suggested by chemical studies of mantle xenoliths.

5.1.2. Thermal conductivity

Thermal conductivity is computed using a P–T-composition dependent model resulting from a combination of lattice and radiative components. Once the total conductivity of each mineral component is estimated, the effective thermal conductivity is computed using a geometric mixing model (Clauser and Huenges, 1995).

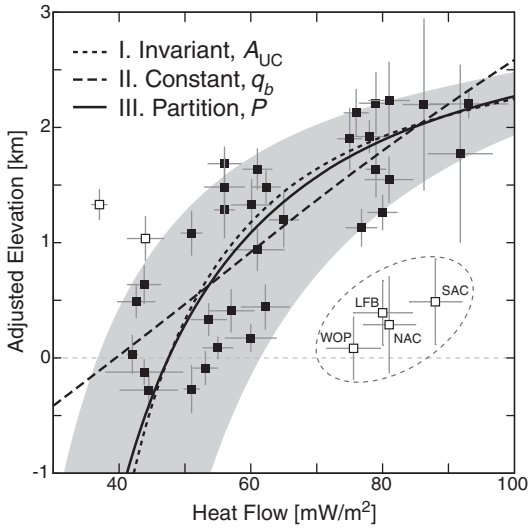

Fig. 3. Best-fitting thermal isostatic models for each of the heat production models. Compositionally adjusted elevation for North American geologic provinces from Hasterok and Chapman (2007b), open squares not used in best-fitting model. The light gray region represents the 95% bounds for data used in the fit, falling between partition coefficients of 0.54 to 1 relative to the partition model $F = 0.74$ with a zero-elevation heat-flow, q_{ref}, of 47.5 mW/m^2. Several provinces with high upper crustal heat production are circled. Abbreviations are as follows: WOP, Wopmay orogen; NAC; North Australian craton; SAC, South Australian craton; and LFB, Lachlan Fold Belt. Modeled elevation for NAC, SAC, and LFB are included in the Supplement Table S.3.

The lattice contribution is computed using a simplified form of Eq. (10) by Hofmeister (1999),

$$\lambda_L(P,T) = \lambda^{\circ}\left(\frac{298}{T}\right)^{n}\left(1 + \frac{K'_T}{K_T}P\right), \tag{8}$$

where T is in Kelvin, λ° is the conductivity at 0 GPa and 298 K, K_T and K'_T are the isothermal bulk modulus and its first pressure derivative, and n is an empirically derived fitting constant. At lithospheric temperatures and pressures, the additional exponential factor included by Hofmeister (1999) is very near unity and thus ignored (Beck et al., 2007). Constants used to compute conductivity are given in Supplement Table S.4.

The radiative contribution to thermal conductivity, λ_R, is negligible at room temperature but represents a significant fraction of the effective conductivity at high temperatures. We use an empirically derived relation for the radiative conductivity developed by Hasterok (2010),

$$\lambda_R(T) = \frac{1}{2}\lambda_{R_{\max}}\left[1 + erf\left(\frac{T - T_R}{\omega}\right)\right], \tag{9}$$

where $\lambda_{R_{\max}}$ is the maximum radiative conductivity, ω is a scaling factor and T_R is the temperature at $0.5\lambda_{R_{\max}}$. For olivine, this estimate is significantly different from previous estimates of the radiative contribution (Hofmeister, 1999, 2005; Shankland et al., 1979). Fig. S.1 of the Supplementary material illustrates our conductivity model.

6. Results and discussion

Aside from temperature measurements in boreholes, a number of other techniques can be used to estimate lithospheric temperatures. Curie depth, base of the seismogenic zone, and elastic thickness constraints have significant uncertainties associated with temperature. Mantle seismic velocities and electrical conductivity estimates are better correlated with temperature (e.g. Goes and van der Lee, 2002; Ledo and Jones, 2005) but are subject to variations from chemical depletion, melting and hydration that can make their interpretation difficult (Poe et al., 2010; Schutt and Lesher, 2006; Yoshino et al.,

2009). Uncertainties for these techniques are often too large for predicting metamorphic reactions, strength of the lithosphere, but may be overcome with additional information (Deen et al., 2006). To overcome these limitations and keep the analysis relatively simple, we use an estimate of the thermal buoyancy which is sensitive to the relative thermal state of the entire lithosphere. To constrain absolute temperatures, xenolith *P–T* estimates provide the range of allowable upper mantle temperatures for a geotherm family and province geotherms in well sampled and thermally steady-state regions.

6.1. Constraint I: thermal isostasy

Much like the subsidence patterns of the oceanic sea-floor that result from the integrated cooling of the lithosphere (e.g., Parsons and Sclater, 1977), continental elevations record a thermal isostatic effect that can be estimated by examining the relationship between compositionally corrected elevation and surface HF (Han and Chapman, 1995; Hasterok and Chapman, 2007a,b). Thermal buoyancy varies with temperature as a consequence of thermal expansion/contraction of the lithosphere, and is therefore expressed in the long-wavelength elevation. In this section, we explore how continental elevation, much like oceanic bathymetry in the marine case, can be used as a constraint on continental geotherms, and consequently on HG models for continental lithosphere.

Unlike the ocean crust where composition is fairly uniform, the compositional buoyancy of the continents is highly variable and must first be removed before the effects for thermal buoyancy may be observed. To estimate the compositional buoyancy, Hasterok and Chapman use seismic derived crustal thickness estimates and empirical seismic velocity to density relations. Each geologic province is then isostatically normalized to account for variations in crustal density and thickness relative to a reference crustal column.

By selecting entire provinces, the effects from short-wavelength flexure on elevation should be minimized. The remaining contributions to adjusted elevation should result from long-wavelength geodynamic support, mantle compositional variations, and differences in lithospheric temperatures. Aside from a few identifiable provinces with obvious perturbations to adjusted elevation and/or anomalous near-surface radiogenic enrichment, there is a rough correlation between elevation and HF that accounts for approximately 2.5 km of elevation (Fig. 3), not unlike the variations in thermal buoyancy of oceanic lithosphere (Hillier and Watts, 2005).

The elevation difference, $\Delta\varepsilon_T$, between two regions can be computed by

$$\Delta\varepsilon_T = \int_0^{z_{max}} \left[\alpha_V(z,T)T(z) - \alpha'_V(z,T)T'(z)\right]\, dz, \tag{10}$$

where T(z) and $T'(z)$ represent lithospheric geotherms and $\alpha_V(z,T)$ is the *P–T* dependent volumetric expansivity computed using the method of Afonso et al. (2005). The primed and unprimed symbols represent the reference and observed columns, respectively. The maximum depth of integration, z_{max}, is the depth at which the coolest geotherm reaches the mantle adiabat. Constants used to estimate expansivity and density are given in Supplement Table S.5. Every set of geotherm model parameters produces a family of geotherms from which a model thermal isostasy curve (elevation versus HF) can be calculated.

To test thermal isostatic models, we use the observed HF and modeled compositionally adjusted elevation – normalized for variations in crustal thickness and density – for 33 tectonic provinces from North America (Tables 2 and 3 from Hasterok and Chapman, 2007b). The Pacific Coast Ranges, Central Valley of California, and some anomalously high HG terranes (e.g. WOP in Fig. 3) are excluded from the fit due to large extraneous influences on the elevation and/or HF (see Hasterok and Chapman, 2007b for discussion). We assume the remaining provinces have little systematic variation in compositional buoyancy or dynamic topography with HF, the adjusted elevations is then used to estimate the variation in the average thermal state between these provinces.

Misfits to compositionally normalized elevations of North America are shown in Fig. 4. The misfit is computed by,

$$\text{Misfit} = \left[\frac{S^2}{N}\sum_{i=1}^{N}\left(q_i - q_m\right)^2 + \frac{1}{N}\sum_{j=1}^{N}\left(\varepsilon_j - \varepsilon_m\right)^2\right]^{1/2}, \tag{11}$$

where N is the number of samples, q_i and q_m are the observed HF and model HF, and ε_i and ε_m are the adjusted province elevation and model elevation, respectively. A standard practice with a multi-parameter misfit functionals is to scale the differences between data and model estimates by the associated uncertainty in each data point. However, the uncertainties in HF and/or adjusted elevation for some provinces are overly optimistic and yield unreasonably large influence on the resulting fit. Therefore, in order to give roughly equal weights to the elevation and HF dimensions, the HF is scaled by, $S = 4$ km/70 mW/m^2, although the exact value is somewhat arbitrary. Results are only shown for upper-crustal HG thickness $D = 16$ km and proton composition mantle (Table 1).

Given the scatter in normalized elevations, it is unsurprising that the misfit surface shows that each model class has a considerable range of reasonable parameters. The minimum misfit for the invariant and partition models are very similar (~0.34) and only slightly higher

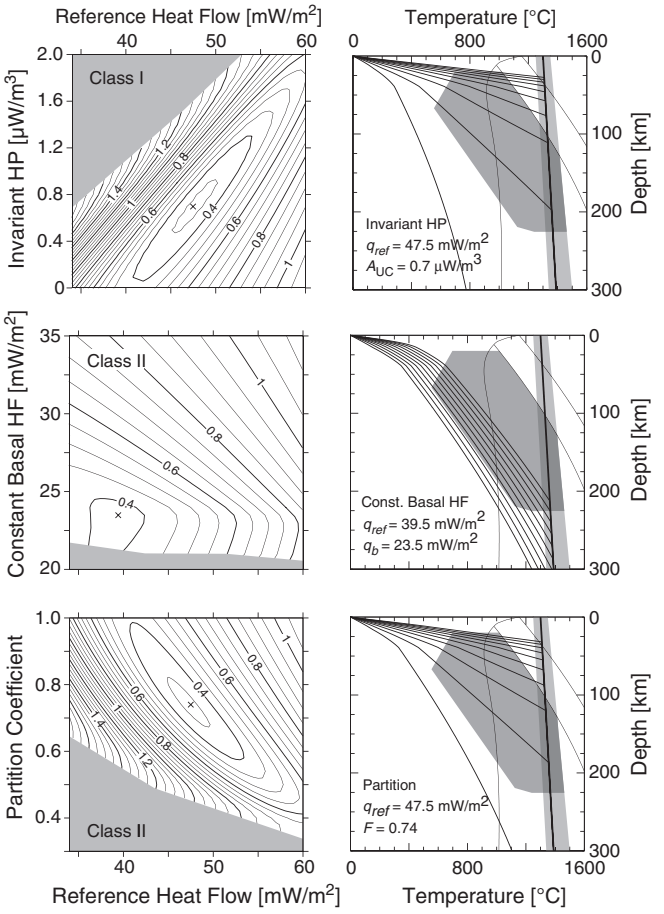

Fig. 4. Misfit of heat production models to compositionally adjusted elevation (left). Best-fit model represented as '×.' Models where the zero-elevation heat flow does not reach the adiabat are shown in gray. Best-fitting geotherms for each associated heat production class (right). Geotherms range from 30 to 120 mW/m^2. Faceted region represents the field of *P–T* estimates from mantle xenoliths (Fig. 5). Melting curves for anhydrous, water-saturated and 50 ppm H_2O (Katz et al. (2003); Fig. 5).

for the constant basal HF model (0.39). Misfits using geotherms from this study show an improvement in fit over previous work using geotherm families computed using the method by Chapman (1986), which have a minimum misfit >0.7 (Hasterok and Chapman, 2007b). The best-fitting thermal isostatic curve for the invariant model has an upper crustal HG of 0.7 μW/m^3 and zero-elevation HF of 47.5 mW/m^2. The elevation resulting from the invariant model over typical values of continental HF is ~2.5 km, and very similar in shape to the partition model (Fig. 3).

The partition model results in the same zero-elevation HF as the invariant model with a partition coefficient of 0.74. This value is slightly higher than a recent global estimate of partition coefficient from Artemieva and Mooney (2001) and higher than our previous estimate of 0.6 using the Chapman (1986) style geotherms. This higher value results from our improved conductivity model and the use of *P–T* dependent thermal expansivity.

The elevation pattern predicted by constant basal HF model is very different from those resulting from the invariant and partition models (Fig. 3), although the range of elevation for observed HF data is similar. Geotherms computed using the Class II model also differ radically from Class I and III (Fig. 4). The minimum misfit has a zero-elevation HF of 39.5 mW/m^2, and a basal HF of 23.5 mW/m^2. Physically, the basal HF is a combination of the sub-lithospheric HF and radiogenic HF from the lower crust and mantle lithosphere. For a 40 mW/m^2 cratonic region, our geotherm models predict a lithospheric thickness of ~200 km, and the total radiogenic contribution from the lower crust and mantle is then 12.4 mW/m^2. Using estimates of sub-lithospheric HF from the Canadian shield (11–15 mW/m^2) (Mareschal and Jaupart, 2004), the predicted lower bound for basal HF is consistent with the best-fitting result.

6.1.1. Effect of varying D

The thickness of the upper crustal HG layer, *D*, need not be the same as the compositional upper crust as some processes such as melt migration and fluid circulation may concentrate HPE's toward the surface (Gosnold, 1987; Jaupart et al., 1981). We have run a series of tests to examine the importance of *D* on total HG estimates, without varying the thickness of the upper crust for other physical properties. Tests varying *D* between 6 and 18 km show that the partition coefficient is relatively insensitive to variations in *D*, ranging from 0.76 at 8 km to 0.74 at 16 km. For Class I models, iso-misfit lines closely track constant values of $A_{UC}D$, implying a nearly constant upper crustal radiogenic HF. Best-fitting upper crustal radiogenic contributions to HF range from 9.9 mW/m^2 at 6 km to 11.2 mW/m^2 at 16 km. These observations do not hold when *D* and the compositional upper crustal thickness are the same. Rather than iso-misfit lines tracking $A_{UC}D$, iso-misfit lines are relatively insensitive to changes in A_{UC} when the upper crustal thickness and *D* variations are coupled.

Independent estimates of *D* range from 2 to 16 km, with an average of ~8–10 km determined using HF–HG relationships (Artemieva and Mooney, 2001). Heat flow–HG relationships were originally developed to explain a relationship between these two parameters for co-genetic plutons (Birch et al., 1968; Förster and Förster, 2000; Gosnold, 1987; Roy et al., 1968) and, although frequently attempted, may not work when extended to encompass all rocks in a given region (Furlong and Chapman, 1987; Jaupart and Mareschal, 1999; Nielson, 1987). The value of *D* determined from HG–HF relationships may also be more sensitive to the lateral scale of HG variations as much or more than the vertical variations, representing a lower bound on the thickness of the upper-crustal HG layer (Jaupart, 1983; Sandiford and McLaren, 2002).

6.1.2. Effect of mantle composition

Archon and Proton mantle compositions produce nearly identical results whereas the Tecton composition fits to elevation result in ~10% higher total HG with similar misfit. The higher HG compensates for conductivity difference between the Archon/Proton and Tecton compositions. This result implies that younger tectonic regions are slightly enriched in upper crustal HPE's than older terranes. The reduction in HPE's with age and affinity for melts that migrate towards the surface in tectonically active regions likely contributes to the greater enrichment in the upper crust of young terranes. However, the conductivities of mantle phases other than olivine and garnet are not well constrained and require further study before these differences in model results can be rigorously modeled.

6.2. Constraint II: xenolith P–T conditions

While thermal elevation contributions can be used to estimate the average difference between geotherms, it is not possible to estimate absolute temperature. However, we can use xenolith *P–T* estimates as constraints on absolute temperature. Estimated temperatures and pressures for 1449 mantle xenoliths are shown in Fig. 5. Temperatures range from 650 to 1500 °C over a range of pressures equivalent to depths of 25 to 225 km. A few xenoliths from the Dabie–Sulu belt appear to be well outside the range of other localities, which reflects rapid subduction of material that did not have time to equilibrate to ambient mantle conditions.

While there is some variation in high temperature and high pressure xenoliths >100 km, temperatures rarely exceed the 1300 °C adiabat. In contrast to the high pressure–high temperature xenoliths, at low pressures there appear to be very few high temperatures above the 50 ppm melting curve (Fig. 5). Either temperatures are buffered by melting, restricting maximum geotherm temperatures to the 50 ppm solidus and not the adiabat, or *P–T* conditions are poorly sampled. Alternatively, these xenoliths may be sampled but *P–T* estimates may not be possible using the Brey and Köhler (1990) thermobarometers. As melting continues to higher melt fractions, clinopyroxene is one of the first minerals to be exhausted (Katz et al., 2003). The removal of solid clinopyroxene makes *T* estimates from the 2-pyroxene thermometers such as T_{BKN} used in this study impossible, suggesting that the lack of data does not preclude the higher temperatures at low pressure. This effect assumes a water concentration >50 ppm.

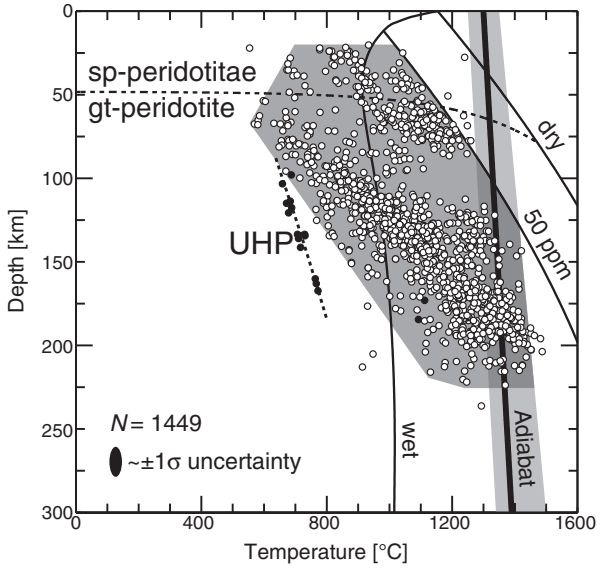

Fig. 5. Estimated *P–T* conditions for mantle xenoliths using the P_{BKN} and T_{BKN} barometer and thermometers (circles). Conditions for the ultra-high pressure Dabie–Sulu belt shown in black (Zheng et al., 2006). Estimated uncertainty for *P–T* estimates (oval $\pm 1\sigma$) is ± 0.3 GPa (~9 km) for pressure and ± 20 K for temperature (Brey and Köhler, 1990). Melting curves by Katz et al. (2003). The heavy black adiabat is represented by a potential temperature of 1300 °C with a gradient of 0.3 °C/km. The estimated spinel–garnet transition is given by the dashed line (Eq. 4).

6.2.1. Xenolith-derived geotherms (xenotherms)

Typical values for regional HF on the continents range from a little less than 40 mW/m^2 to ~100 mW/m^2 and can reach 120 mW/m^2 in magmatic provinces and active rift zones. In cases of extremely low crustal HP the conductive HF can be as low as ~20 mW/m^2 (Chapman and Pollack, 1974; Mareschal et al., 2000; Roy and Rao, 2000). The best-fitting geotherm family for the constant basal HF model (Fig. 4 middle panel) is cooler than the xenolith *P–T* field at low HF and does not reach the high temperatures recorded by xenoliths at intermediate and low pressures. Both the invariant and partition models appear to fall within the range of xenolith *P–T* field. The temperatures for the 40–120 mW/m^2 geotherms are relatively similar. For a HF of 30 mW/m^2, neither geotherm family reaches the 1300 °C adiabat by 300 km. However, at 30 mW/m^2 the two geotherm models diverge considerably with a difference of ~350 K at 300 km.

In addition to examining the full *P–T* field from mantle xenoliths, we model the HF for 10 individual kimberlite provinces that we assume are near thermal steady-state conditions. Geotherms are computed using our preferred geotherm model, $F=0.74$, with an Archon composition. Misfit for these xenotherms (xenolith-derived geotherms) is computed using the misfit functional,

$$\text{misfit} = \left[\frac{1}{N}\sum_{i=0}^{N}\left(\frac{\delta T_i^2}{\sigma_T^2} + \frac{\delta P_i^2}{\sigma_P^2}\right)\right]^{-1/2}, \quad (12)$$

where δT_i and δP_i are the differences between the geotherm and xenolith *P–T* conditions. The differences are normalized by the estimated uncertainties in xenolith *P–T* results from the geobarometer P_{BKN} ($\sigma_P=0.3$ GPa) and T_{BKN} ($\sigma_T=20$ K) (Brey and Köhler, 1990).

Using our reference HG model to fit the xenolith *P–T* conditions we estimate a surface HF of 40.2 mW/m^2 for the Kalahari craton (Fig. 6). This HF is somewhat lower than other estimates from the Kalahari craton (Jones, 1988, 1992; Nicolaysen et al., 1981). However, one must be cautious when making comparisons of present day surface HF with those at the time of kimberlite eruptions as thermal perturbations at the base of a 200 km thick lithosphere can take on the order of 300 m.y. to reach the surface. The variations in HF at the surface can result from a combination of HG variations within the shallow upper crust and differential heating in space and time at the base of the lithosphere.

Xenolith *P–T* estimates for the Kalahari craton come from a number of geographically separated localities and while there may be some small variations in *P–T* distributions (Bell et al., 2003), they show a significant overlap without accounting for uncertainties in the geothermobarometers. The temperature variations could result from steady-state thermal refraction due to lateral differences in composition. At $_?\gtrsim$5 GPa beneath the Kalahari craton there is a documented increase in the scatter of *P–T* estimates possibly related to non-steady state thermal conditions (Bell et al., 2003). This scatter occurs within the diamond stability field (i.e. source region for the kimberlite eruptions). However, the fit to geotherms is not considerably different than those needed to model the data above 5 GPa.

Fig. 7 shows best-fitting geotherms to *P–T* estimates of the remaining nine xenolith provinces. Xenotherm misfits range from ~3 to 5 with a surface HF uncertainty of ±2 mW/m^2 estimated from the width of the misfit trough. The xenotherm fits indicate that, at the time of xenolith equilibration, HF for the regions analyzed ranged from ~37 to 43 mW/m^2 with an average of 40 mW/m^2. This result is consistent with HF collected in these and other Precambrian cratonic and shield regions (Alexandrino and Hamza, 2008; Mareschal and Jaupart, 2004; Nyblade, 1999; Roy and Rao, 2000; Roy et al., 2008; Sass and Lachenbruch, 1979). Results using the invariant HG are comparable.

To illustrate how the preferred model can then be used to identify radiogenic anomalies, consider the Slave craton. Observed HF on the Slave craton may be high relative to other Archean regions. A single

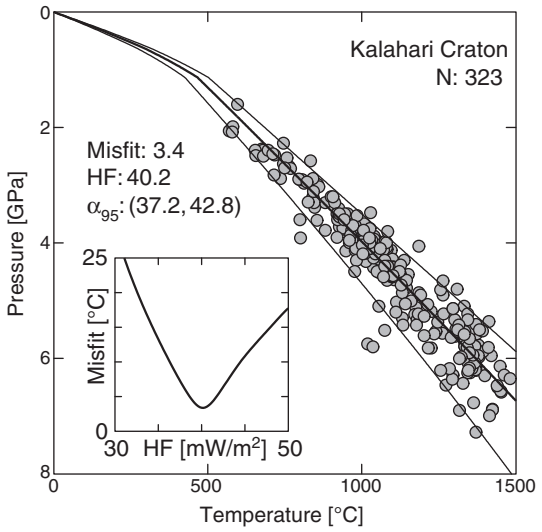

Fig. 6. A member of the preferred geotherm family ($F=0.74$) fit to xenolith *P–T* estimates for the Kalahari craton. Misfit (inset) for variations in surface heat flow (HF) in mW/m^2 computed using Eq. (12). Heavy line represents best-fitting model and light lines represent 95% confidence intervals, α_{95}.

borehole near Yellowknife recorded a HF of ~53 mW/m^2 (Lewis and Wang, 1992) and two boreholes in the Lac de Gras area, near the kimberlite data shown in Fig. 7, yield HF estimates of 43 and 46 mW/m^2 (Mareschal et al., 2004). Using subsets of the xenolith data here, Russell et al. (2001) invert for Moho HF, mantle HG, and temperatures at the base of the mantle. Russell et al. estimate a Moho HF of 15 mW/m^2 and suggest this supports a surface HF >50 mW/m^2 based on observations of anomalously high HG in surface samples. For comparison, we obtain a slightly higher estimate of mantle HF beneath the Slave craton using our reference HG model (~18 mW/m^2).

The observations of high surface HF of the Slave craton suggest that it, like Wopmay orogen to the west, has elevated HF due to above average HG in a thin layer in the uppermost crust (Lewis et al., 2003). Because the thickness of this higher than average (as compared to our preferred model) HG layer is thin, the effect on the geotherm is minimal but will cause a high surface HF. As a consequence, the HF estimated using our best fit to the xenolith *P–T* data will be lower than the observed surface HF. If the HG layer is thin, the difference (~6–16 mW/m^2) between the observed HF and our prediction can be used to estimate the anomalous HG within this layer, assuming one also knows the thickness of the anomalous HG layer.

6.3. Preferred geotherm family

The constant basal HF model is excluded as a viable geotherm family on the basis of its inability to explain global variations in mantle xenolith *P–T* conditions. Elevation and xenolith *P–T* conditions, however, do not discriminate between the invariant and partition models. However, there are a number of factors that suggest a partitioning model is more likely.

In general, HG is higher in younger terranes (Jaupart and Mareschal, 2003), making the constant HG model unlikely. In the Canadian Shield, much of the variation in surface HF can be tied to regional differences in HG (Mareschal and Jaupart, 2004). We estimate the apparent HF of most Precambrian regions is ~40 mW/m^2 as shown by the xenotherm fits above. There are, however, a number of shields and cratons with high HF yet little or no tectonic activity for >1 Ga. This suggests significant variations in near surface HG (Lewis et al., 2003; McLaren et al., 2005).

In light of these observations and our results, our preferred geotherm and HG model is a partition model with ratio of 74:26 between

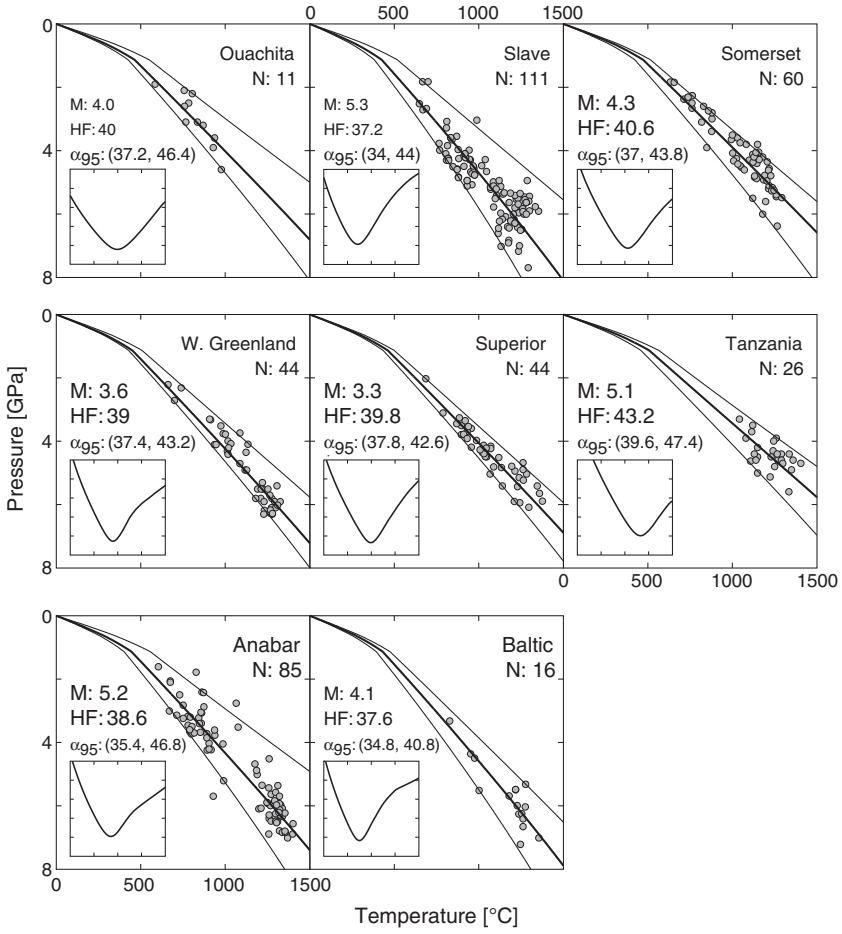

Fig. 7. Fits of preferred geotherm family ($F=0.74$) to xenolith P–T estimates for selected cratonic localities. All inset misfit axes are the same as in Fig. 6. All xenolith P–T conditions use T_{BKN} and P_{BKN} thermobarometers unless noted. Heavy line represents best-fitting model and light lines represent 95% confidence intervals, α_{95}. References for individual cratons are given in Supplement Table S.1 with ages of individual eruptions in Table S.2.

the basal HF and upper crustal radiogenic HF, and an upper-crustal HG thickness of 16 km (Fig. 8).

While we have assumed steady-state conditions, the relaxation time for heat deep within the lithosphere, particularly for shields and cratons, to reach the surface is a significant fraction of the time scales for decay of HPE's. Geotherm models accounting for this effect (Michaut and Jaupart, 2004) show that by assuming a steady-state geotherm, we are over-estimating the present day HG in shields and cratons (Jaupart and Mareschal, 2007). However, the "true" thermal regime is sufficiently similar to a steady-state geotherm that the HG may be regarded as an "apparent" HG rather than "true" HG. The effect on thermally young terranes (<500 Ma) should be relatively minor.

While the results presented in this study represent generalized geotherms and HG distributions, local knowledge can be used to determine locality specific geotherms. For example, the Wopmay orogen of Arctic Canada has a high HF (>75 mW/m^2, Lewis et al., 2003), but also has very high surface HG (est. 4.8 μW/m^3, Lewis et al., 2003). Because this region has experienced very little tectonic activity for the past ~2 Ga, there is no reason to suspect that the high HF is due to recent tectonic activity. Accounting for the high surface HG, geotherm estimates for the Wopmay orogen are more consistent with a shield geotherm than a tectonically active terrane (Hasterok and Chapman, 2007b; Lewis et al., 2003).

This concentrated upper crustal HG can also be found in North and South Australian cratons and the Lachlan fold belt (this study, McLaren et al., 2005), which have elevations, and presumably geotherms, more similar to our thermal isostatic estimate from the 50 mW/m^2 geotherm (Fig. 3). Likewise, we expect the regions with anomalously low surface HF resulting from low crustal HG such as central Africa, northern Superior craton, and Southern Granulite Terrane of India (Chapman and Pollack, 1974; Mareschal et al., 2000; Roy and Rao,

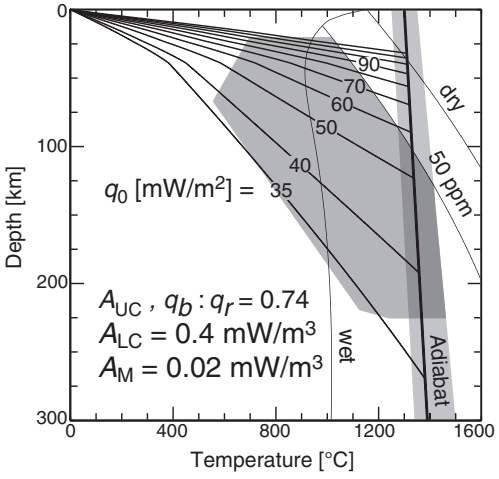

Fig. 8. Preferred geotherm family using the partition model. Other lines and shaded regions are discussed in Fig. 5.

2000) to have elevations and geotherms similar to our 40 mW/m^2 geotherm.

6.4. Lithospheric thickness and sub-lithospheric heat flow

Many geodynamic processes require an estimate of lithospheric thickness and/or the HF at the base of the lithosphere. Values for these parameters can be derived from the preferred geotherm models (Fig. 9). Lithospheric thickness ranges from just under 200 km at 40 mW/m^2 surface HF to ~50 km at 90 mW/m^2.

Geotherms no longer intersect the adiabat for HF <34 mW/m^2. Sub-lithospheric HF is estimated by subtracting the estimated upper crustal HG from the partition model and the contributions from the lower crust and mantle lithosphere. Minimum sub-lithospheric HF for the preferred geotherm family is 11 mW/m^2 and increases to just under 65 mW/m^2 for a 100 mW/m^2 surface HF. The sub-lithospheric HF is nearly linear despite the large curvature in the lithospheric thickness because HG within the mantle is very small in our models. However, one must be somewhat cautious using only surface HF to estimate the Moho and sub-lithospheric HF as the same regions with highly anomalous upper crustal HG will yield poor estimates of sub-lithospheric HF using this method.

Using surface HF models from xenotherms (Figs. 6 and 7), one can estimate the range of sub-lithospheric HF into shields and cratons (14.5–20 mW/m^2). Including the radiogenic contribution from the mantle lithosphere, the range of Precambrian Moho HF is 18–23 mW/m^2, consistent with the upper end of the range of estimated for a number of shields and cratons (7–25 mW/m^2) (Jaupart et al., 2007).

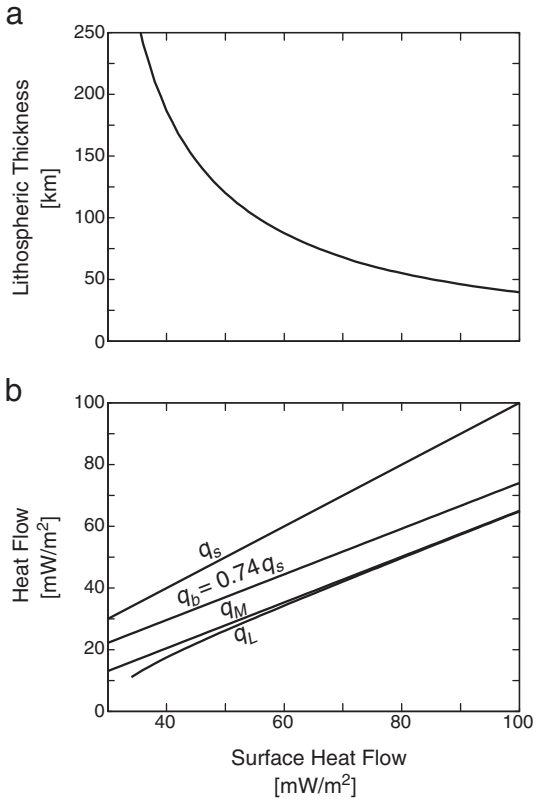

Fig. 9. Lithospheric thickness and heat loss. (a) Lithospheric thickness for the partition model with coefficient $F = 0.74$, and proton mantle composition. (b) Heat flow across lithospheric layers: surface, q_s; middle to upper crust, q_b; Moho, q_M; and lithosphere–asthenosphere boundary, q_L.

7. Conclusions

Radiogenic heat generation (HG) is highly variable within the continental lithosphere and difficult to estimate from standard geophysical techniques. Compositionally corrected elevations and xenolith thermobarometry can be used to reduce substantially the uncertainties in upper crustal HG. We define three types of HG models: an invariant HG (independent of surface heat flow (HF)); constant basal HF below the radiogenically enriched upper crust; and partitioning between upper crustal radiogenic HG and basal HF. Xenolith *P–T* estimates suggest the constant basal HF models are not generally applicable. Likewise surface observations of HG suggest upper crustal HG can not be invariant.

We propose a reference HG model for the continental lithosphere with 26% of the surface HF resulting from upper-crustal HG within a 16 km thick layer. Lower crustal and lithospheric mantle HG are estimated at 0.4 and 0.02 μW/m^3, respectively. Our model is calibrated using compositionally normalized elevation for 33 individual tectonic provinces in North America and verified with xenolith *P–T* suites from 10 separate cratons and shields worldwide. Our preferred geotherm family estimates HF between 37 and 43 mW/m^3 for these Precambrian xenoliths with a corresponding lithospheric thickness between 225 and 135 km, respectively. Predicted sub-lithospheric HF for these localities varies from 14.5 to 20 mW/m^2.

Supplementary materials related to this article can be found online at doi:10.1016/j.epsl.2011.04.034.

Acknowledgments

We would like to thank R. Rudnick and D. Bell for sharing their xenolith *P–T* databases. We would also like to thank Y. Ricard, S. Roy, and an anonymous reviewer for their suggestions that significantly improved the manuscript as well as the FoLK group at Utah especially P. Gettings and M.G. Davis for their helpful discussions along the way. Funding for D. Hasterok was provided by the Department of Geology and Geophysics at the University of Utah.

References

Ackerman, L., Mahlen, N., Jelínek, E., Medaris, G., Ulrych, J., Strnad, L., Mihaljevič, M., 2007. Geochemistry and evolution of subcontinental lithospheric mantle in central Europe: evidence from peridotite xenoliths of the Kozákov volcano, Czech Republic. J. Petrol. 48, 2235–2360.

Afonso, J., Ranalli, G., Fernàndez, M., 2005. Thermal expansivity and elastic properties of the lithospheric mantle: results from mineral physics of composites. Phys. Earth Planet. Inter. 149, 279–306.

Alexandrino, C., Hamza, V., 2008. Estimates of heat flow and heat production and a thermal model of the São Francisco craton. Int. J. Earth Sci. 97, 289–306.

Allis, R., 1979. A heat production model for stable continental crust. Tectonophysics 57, 151–165.

Artemieva, I., Mooney, W., 2001. Thermal thickness and evolution of Precambrian lithosphere: a global study. J. Geophys. Res. 106, 16387–16414.

Ashwal, L., Morgan, P., Kelley, S., Percival, J., 1987. Heat production in an Archean crustal profile and implications for heat flow and mobilization of heat-producing elements. Earth Planet. Sci. Lett. 85, 439–450.

Attoh, K., Morgan, J., 2004. Geochemistry of high-pressure granulites from the Pan-African Dahomeyide orogen, West Africa: constraints on the origin and composition of the lower crust. J. Afr. Earth. Sci. 39, 201–208.

Balling, N., Eriksson, K., Landstroem, O., Lind, G., Malmquist, D., 1990. Naturgas, Vattenfall, 57.

Beck, P., Goncharov, A., Struzhkin, V., Militzer, B., Mao, H., Hemley, R., 2007. Measurement of thermal diffusivity at high pressure using a transient heating technique. Appl. Phys. Lett. 91, 181914.

Bell, D., Rossman, G., Maldener, J., Endisch, D., Rauch, F., 2003. Hydroxide in olivine: a quantitative determination of the absolute amount and calibration of the IR spectrum. J. Geophys. Res. 108. doi:10.1029/2001JB000679.

Bianchini, G., Beccaluva, L., Bondaiman, C., Nowell, G., Pearson, G., Siena, F., Wilson, M., 2007. Evidence of diverse depletion and metasomatic events in harzburgite–lherzolite mantle xenoliths from the Iberian plate (Olot, NE Spain): implications for lithosphere accretionary processes. Lithos 94, 25–45.

Birch, F., Roy, R., Decker, E., 1968. Heat flow and thermal history in New England and New York. In: Zen, E., White, W.S., Hadley, J.B., Thompson, J.B., et al. (Eds.), Studies of Appalachian Geology: Northern and Maritime. Interscience, New York, pp. 437–451.

Bjerg, E., Ntaflos, T., Kurat, G., Dobosi, G., Labudía, C., 2005. The upper mantle beneath Patagonia, Argentina, documented by xenoliths from alkali basalts. J. South Am. Earth Sci. 18, 125–145.
Bodorkos, S., Sandiford, M., Minty, B., Blewett, R., 2004. A high-resolution, calibrated airborne radiometric dataset applied to the estimation of crustal heat production in the Archean northern Pilbara Craton, Western Australia. Precambrian Res. 128, 57–82.
Brady, R., Ducea, M., Kidder, S., Saleeby, J., 2006. The distribution of radiogenic heat production as a function of depth in the Sierra Nevada Batholith, California. Lithos 86, 229–244.
Brey, G., Köhler, T., 1990. Geothermobarometry in four-phase lherzolites II. new thermobarometrs, and practical assessment of existing thermobarometers. J. Petrol. 31, 1353–1378.
Chapman, D., 1986. Thermal gradients in the continental crust. In: Dawson, J., Carswell, D., Hall, J., Wedepohl, K. (Eds.), The Nature of the Lower Continental Crust: Geol. Soc. Spec. Pub., No. 24, pp. 63–70. Denver.
Chapman, D., Pollack, H., 1974. Cold spot in West Africa: anchoring the African plate. Nature 250, 477–478.
Christensen, N., Mooney, W., 1995. Seismic velocity structure and composition of the continental crust: a global view. J. Geophys. Res. 100, 9761–9788.
Clauser, C., Huenges, E., 1995. Thermal conductivity of rocks and minerals. In: Ahrens, T. (Ed.), Rock Physics and Phase Relations: a Handbook of Physical Constants. : of AGU Reference Shelf, 3. AGU, Washington, D.C., pp. 105–126.
Clauser, C., Giese, P., Huenges, E., Kohl, T., Lehmann, H., Rybach, L., Safanda, J., Wilhelm, H., Windloff, K., Zoth, G., 1997. The thermal regime of the crystalline continental crust: implications from the KTB. J. Geophys. Res. 102, 18417–18441.
Deen, T., Griffin, W., Begg, G., O'Reilly, S., Natapov, L., Hronsky, J., 2006. Thermal and compositional structure of the subcontinental lithospheric mantle: derivation from shear wave seismic tomography. Geochem. Geophys. Geosyst. 7, Q07003.
Del Lama, E., de Oliveira, M., Zanardo, A., 1998. Geochemistry of the Guaxupé granulites, Minas Gerias, Brazil. Gondwana Res. 6, 357–365.
Dziewonski, A.M., Anderson, D.L., 1981. Preliminary reference earth model. Phys. Earth Planet. Inter. 25 (4), 297–356.
Flowers, R., Royden, L., Bowring, S., 2004. Isostatic constraints on the assembly, stabilization, and preservation of cratonic lithosphere. Geology 32, 321–324.
Förster, A., Förster, H., 2000. Crustal composition and mantle heat flow: implications from surface heat flow and radiogenic heat production in the Variscan Erzgebirge (Germany). J. Geophys. Res. 105, 27917–27938.
Fountain, D., Salisbury, M., Furlong, K., 1987. Heat production and thermal conductivity of rocks from the Pikwitonei–Sachigo continental cross section, central Manitoba: implications for the thermal structure of the Archean crust. Can. J. Earth Sci. 24, 1583–1594.
Furlong, K., Chapman, D., 1987. Crustal heterogeneities and the thermal structure of the continental crust. Geophys. Res. Lett. 14, 314–317.
Furukawa, Y., Shinjoe, H., 1997. Distribution of radiogenic heat generation in the arc's crust of Hokkaido Island, Japan. Geophys. Res. Lett. 24, 1279–1282.
Garrido, C., Bodinier, J., Burg, J., Zeilinger, G., Hussain, S., Dawood, H., Chaudhry, M., Gervilla, F., 2006. Petrogenesis of mafic garnet granulite in the lower crust of the Kohistan paleo-arc complex (northern Pakistan): implications fro intra-crustal differentiation of island arcs and generation of continental crust. J. Petrol. 47, 1873–1914.
Goes, S., van der Lee, S., 2002. Thermal structure of the North American uppermost mantle inferred from seismic tomography. J. Geophys. Res. 107.
Gosnold, W., 1987. Redistribution of U and Th in shallow plutonic environments. Geophys. Res. Lett. 14, 291–294.
Griffin, W., O'Reilly, S., Ryan, C., 1999. The composition and origin of sub-continental lithospheric mantle. In: Fei, Y., Bertka, C., Mysen, B. (Eds.), Mantle Petrology: Field Observations and High Pressure Experimentation: a Tribute to Francis R. (Joe) Boyd. Special Publication: Geochem. Soc., St. Louis, MO, 6, pp. 13–45.
Han, U., Chapman, D., 1995. Thermal isostasy: elevation changes of geologic provinces. J. Geol. Soc. Korea 31, 106–115.
Hanley, E., Dewitt, D., Roy, R., 1978. The thermal diffusivity of eight well-characterized rocks for the temperature range 300–1000 K. Eng. Geol. 12, 31–47.
Hasterok, D., 2010. Thermal state of the oceanic and continental lithosphere. Ph.D. thesis, University of Utah.
Hasterok, D., Chapman, D., 2007a. Continental thermal isostasy I: methods and sensitivity. J. Geophys. Res. 112. doi:10.1029/2006JB004663.
Hasterok, D., Chapman, D., 2007b. Continental thermal isostasy II: applications to North America. J. Geophys. Res. 112. doi:10.1029/2006JB004664.
Hawkesworth, C., 1974. Vertical distribution of heat production in the basement of the eastern Alps. Nature 249, 435–436.
He, L., Hu, S., Huang, S., Yang, W., Wang, J., Yuan, Y., Yang, S., 2008. Heat flow study at the Chinese Continental Scientific Drilling site: borehole temperature, thermal conductivity, and radiogenic heat production. J. Geophys. Res. 113, B02404.
Hillier, J., Watts, A., 2005. Relationship between depth and age in the North Pacific Ocean. J. Geophys. Res. 110, B02405.
Hofmeister, A., 1999. Mantle values of thermal conductivity and the geotherm from phonon lifetimes. Science 283, 1699–1706.
Hofmeister, A., 2005. Dependence of diffusive radiative transfer on grain-size, temperature, and Fe-content: implications for mantle processes. J. Geodyn. 40, 51–72.
Hölttä, P., 1997. Geochemical characteristics of granulite facies rocks in the Archean Varpaisjärvi area, central Fennoscandian Shield. Lithos 40, 31–53.
Hyndman, R., Currie, C., Mazzotti, S., 2005. Subduction zone backarcs, mobile belts, and orogenic heat. GSA Today 15, 4–10.
Ionov, D., 2004. Chemical variations in peridotite xenoliths from Vitim, Siberia: inferences for REE and Hf behaviour in the garnet-facies upper mantle. J. Petrol. 45, 343–367.
Ionov, D., Ashchepkov, I., Stosch, H.-G., Witt-Eickschen, G., Seck, H., 1993. Garnet peridotite xenoliths from the Vitim volcanic field, Baikal region: the nature of the garnet-spinel peridotite zone in the continental mantle. J. Petrol. 34, 1141–1175.
Ionov, D., O'Reilly, S., Genshaft, Y., Kopylova, M., 1996. Carbonate-bearing mantle peridotite xenoliths from Spitsbergen: phase relationships, mineral compositions and trace-element residence. Contrib. Mineral. Petrol. 125, 375–392.
Ionov, D., Bodinier, J.-L., Mukasa, S., Zanetti, A., 2002. Mechanisms and sources of mantle metasomatism: major and trace element compositions of peridotite xenoliths from Spitsbergen in the context of numerical modelling. J. Petrol. 43, 2219–2259.
Ionov, D., Chanefo, I., Bodinier, J., 2005. Origin of Fe-rich lherzolite and wehrlites from Tok, SE Siberia by reactive melt percolation in refractory mantle peridotites. Contrib. Mineral. Petrol. 150, 335–353.
Jaupart, C., 1983. Horizontal heat transfer due to radioactivity contrasts: causes and consequences of the linear heat flow relation. Geophys. J. R. Astron. Soc. 75, 411–435.
Jaupart, C., Mareschal, J., 1999. The thermal structure and thickness of continental roots. Lithos 48, 93–114.
Jaupart, C., Mareschal, J.-C., 2003. Constraints on crustal heat production from heat flow data. In: Rudnick, R. (Ed.), Treatise on Geochemistry: the Crust., Vol. 3. Elsevier, pp. 65–84. Ch. 2.
Jaupart, C., Mareschal, J.-C., 2007. Heat flow and thermal structure of the lithosphere. In: Shubert, G., Watts, A. (Eds.), Treatise on Geophysics: Crust and Lithospheric Dynamics., Vol.6. Elsevier, pp. 217–251. Ch. 5.
Jaupart, C., Sclater, J., Simmons, G., 1981. Heat flow studies: constraints on the distribution of uranium, thorium and potassium in the continental crust. Earth Planet. Sci. Lett. 52, 328–344.
Jaupart, C., Labrosse, S., Mareschal, J.-C., 2007. Temperatures, heat and energy in the mantle of the Earth. In: Shubert, G., Bercovici, D. (Eds.), Treatise on Geophysics: Mantle Dynamics., Vol. 7. Elsevier, pp. 253–303. Ch. 6.
Jõeleht, A., Kukkonen, I., 1998. Thermal properties of granulite facies rocks in the Precambrian basement of Finland and Estonia. Tectonophysics 291, 195–203.
Jones, M., 1988. Heat flow in the Witwatersrand Basin and environs, and its significance for the South African shield geotherm and lithospheric thickness. J. Geophys. Res. 93, 3243–3260.
Jones, M., 1992. Heat flow anomaly in Lesotho: implications for the southern boundary of the Kaapvaal craton. Geophys. Res. Lett. 19, 2031–2034.
Katz, R., Spiegelman, M., Langmuir, C., 2003. A new parameterization of hydrous mantle melting. Geochem. Geophys. Geosyst. 9, 1073.
Ketcham, R., 2006. Distribution of heat-producing elements in the upper and middle crust of southern and west central Arizona: evidence from core complexes. J. Geophys. Res. 101, 13611–13632.
Klemme, S., O'Neill, H., 2000. The near-solidus transition from garnet lherzolite to spinel lherzolite. Contrib. Mineral. Petrol. 138, 237–248.
Kukkonen, I., Jõeleht, A., 1996. Geothermal modelling of the lithosphere in the central Baltic Shield and its southern slope. Tectonophysics 255, 25–45.
Kukkonen, I., Lahtinen, R., 2001. Variation of radiogenic heat production rate in 2.8–1.8 Ga old rocks in the central Fennoscandian Shield. Phys. Earth Planet. Inter. 126, 279–294.
Lachenbruch, A., 1968. Preliminary geothermal model of the Sierra Nevada. J. Geophys. Res. 73, 6977–6989.
Lachenbruch, A., 1970. Crustal temperature and heat production: implications for the linear heat flow relation. J. Geophys. Res. 75, 3291–3300.
Lachenbruch, A., Bunker, C., 1971. Vertical gradients of heat production in the continental crust: 2. some estimates from borehole data. J. Geophys. Res. 76, 3852–3860.
Ledo, J., Jones, A., 2005. Upper mantle temperature determined from combining mineral composition, electrical conductivity laboratory studies and magnetotelluric field observations: application to the intermontane belt, northern Canadian Cordillera. Earth Planet. Sci. Lett. 236, 258–268. doi:10.1016/j.epsl.2005.01.044.
Lewis, T., Wang, K., 1992. Influence of terrain on bedrock temperatures. Palaeogeogr. Palaeoclimatol. Palaeoecol. 98, 87–100.
Lewis, T., Hyndman, R., Flück, P., 2003. Heat flow, heat generation, and crustal temperatures in the northern Canadian Cordillera: thermal control of tectonics. J. Geophys. Res. 108, 2316. doi:10.1029/2002JB002090.
Mareschal, J., Jaupart, C., 2004. Variations of surface heat flow and lithospheric heat production beneath the North American Craton. Earth Planet. Sci. Lett. 223, 65–77.
Mareschal, J., Poirier, A., Rolandone, F., Bienfait, G., Gariépy, C., Lapointe, R., Jaupart, C., 2000. Low mantle heat flow at the edge of the North American continent, Voisey Bay, Labrador. Geophys. Res. Lett. 27, 823–826.
Mareschal, J., Nyblade, A., Perry, H., Jaupart, C., Bienfait, G., 2004. Heat flow and deep lithospheric thermal structure at Lac de Gras, Slave Province, Canada. Geophys. Res. Lett. 31, L12611. doi:10.1029/2004GL020133.
Martignole, J., Martelat, J., 2005. Proterozoic dykes as monitors of HP granulite facies metamorphism in the Grenville Front Tectonic Zone (western Quebec). Precambrian Res. 138, 183–207.
McKenzie, D., 1978. Some remarks on the development of sedimentary basins. Earth Planet. Sci. Lett. 40, 25–32.
McLaren, S., Sandiford, M., Hand, M., Neumann, N., Wyborn, L., Bastrakova, I., 2003. The hot south continent: heat flow and heat production in Australian Proterozoic terranes. J. Geol. Soc. Aust. Spec. Publ. 22, 151–161.
McLaren, S., Sandiford, M., Powell, R., 2005. Contrasting styles of Proterozoic crustal evolution: a hot-plate tectonic model for Australian terranes. Geology 33, 673–676.
Michaut, C., Jaupart, C., 2004. Nonequilibrium temperatures and cooling rates in thick continental lithosphere. Geophys. Res. Lett. 31, L24602.
Nicolaysen, L., Hart, R., Gale, N., 1981. The Vredefort radioelement profile extended to supracrustal strata at Carletonville, with implications for continental heat flow. J. Geophys. Res. 86, 10653–10661.

Nielson, S., 1987. Steady state heat flow in a random medium and the linear heat flow–heat production relationship. Geophys. Res. Lett. 14, 318–321.
Nyblade, A., 1999. Heat flow and the structure of Precambrian lithosphere. Lithos 48, 81–91.
O'Reilly, S., Griffin, W., 2000. Apatite in the mantle: implications for metasomatic processes and high heat production in Phanerozoic mantle. Lithos 53, 217–232.
O'Reilly, S., Griffin, W., Morgan, P., Ionov, D., Horman, M., 1997. Mantle apatite revisited: major reservoir for U and Th in the mantle and reflector of mantle-fluid sources. LPI Contrib. 921, 154.
Owen, J., Longstaffe, F., Greenough, J., 2003. Petrology of sapphirine granulite and associated sodic gneisses from the Indian Head Range, Newfoundland. Lithos 68, 91–114.
Parsons, B., Sclater, J., 1977. An analysis of the variation of ocean floor bathymetry and heat flow with age. J. Geophys. Res. 82, 803–827.
Peltonen, P., Huhma, H., Tyni, M., Shimizu, N., 1999. Garnet peridotite xenoliths from kimberlites of Finland: nature of the continental mantle at an Archean Craton – Proterozoic mobile belt transition. 7th Intl. Kimberlite Conf.
Pinet, C., Jaupart, C., 1987. The vertical distribution of radiogenic heat production in the precambrian crust of Norway and Sweden: geothermal implications. Geophys. Res. Lett. 14, 260–263.
Poe, B., Ramano, C., Nestola, F., Smyth, J., 2010. Electrical conductivity anisotropy of dry and hydrous olivine at 8 GPa. Phys. Earth Planet. Inter. 181, 103–111.
Poirier, J.-P., Tarantola, A., 1998. A logarithmic equation of state. Phys. Earth Planet. Inter. 109, 1–8.
Pollack, H., Chapman, D., 1977. Mantle heat flow. Earth Planet. Sci. Lett. 34, 174–184.
Popov, Y., Pevzner, S., Pimenov, V., Romushkevich, R., 1999. New geothermal data from the Kola superdeep well SG-3. Tectonophysics 306, 345–366.
Rao, R., Rao, G., Reddy, G., 1982. Age dependence of continental heat flow—fantasy and facts. Earth Planet. Sci. Lett. 59, 288–302.
Ray, L., Kumar, P., Reddy, G., Roy, S., Rao, G., Srinivasan, R., Rao, R., 2003. High mantle heat flow in a Precambrian granulite province: evidence from Southern India. J. Geophys. Res. 108. doi:10.1029/2001JB000688.
Ray, L., Förster, H.-J., Schilling, F., Förster, A., 2006. Thermal diffusivity of felsic to mafic granulites at elevated temperatures. Earth Planet. Sci. Lett. 251, 241–253.
Robinson, J., Wood, B., 1998. The depth of the spinel to garnet transition at the peridotite solidus. Earth Planet. Sci. Lett. 164, 277–284.
Roy, S., Rao, R., 2000. Heat flow in the Indian shield. J. Geophys. Res. 105, 25587–25604.
Roy, R., Blackwell, D., Birch, F., 1968. Heat generation of plutonic rocks and continental heat flow provinces. Earth Planet. Sci. Lett. 5, 1–12.
Roy, S., Ray, L., Bhattacharya, A., Srinivasan, R., 2008. Heat flow and crustal thermal structure in the Late Archaean Clospet granite batholith, south India. Int. J. Earth Sci. 97, 245–256.
Rudnick, R., Fountain, D., 1995. Nature and composition of the continental crust: a lower crustal perspective. Rev. Geophys. 33, 267–309.
Rudnick, R., Gao, S., 2003. Composition of the continental crust. In: Rudnick, R. (Ed.), Treatise on Geochemistry: the Crust., Vol. 3. Elsevier, pp. 1–64. Ch. 1,.
Rudnick, R., Nyblade, A., 1999. The thickness and heat production of Archean lithosphere: constraints from xenolith thermobarometry and surface heat flow. In: Fei, Y., Bertka, C., Mysen, B. (Eds.), Mantle Petrology: Field Observations and High Pressure Experimentation: a Tribute to Francis R. (Joe) Boyd. Special Pub: Geochem. Soc., 6.
Rudnick, R., McDonough, W., O'Connell, R., 1998. Thermal structure, thickness and composition of continental lithosphere. Chem. Geol. 145, 395–411.
Rudnick, R., Gao, S., Ling, W., Liu, Y., McDonough, W., 2004. Petrology and geochemistry of spinel peridotite xenoliths from Hannuoba and Qixia, North China craton. Lithos 77, 609–637.
Russell, J., Dipple, G., Kopylova, M., 2001. Heat production and heat flow in the mantle lithosphere, Slave craton, Canada. Phys. Earth Planet. Inter. 123, 27–44.
Rybach, L., Buntebarth, G., 1984. The variation of heat generation, density and seismic velocity with rock type in the continental lithosphere. Tectonophysics 103, 335–344.
Sandiford, M., McLaren, S., 2002. Tectonic feedback and the ordering of heat producing elements within the continental lithosphere. Earth Planet. Sci. Lett. 204, 133–150.
Sass, J., Lachenbruch, A., 1979. Thermal regime of the Australian continental crust. In: McElhinny, M. (Ed.), The Earth: its Origin, Structure and Evolution. Academic Press, London, pp. 301–351.
Schneider, R., Roy, R., Smith, A., 1987. Investigations and interpretations of the vertical distribution of U, Th, and K: South Africa and Canada. Geophys. Res. Lett. 14, 264–267.
Schutt, D., Lesher, C., 2006. Effects of melt depletion on the density and seismic velocity of garnet and spinel lherzolite. J. Geophys. Res. 111. doi:10.1029/2003JB002950.
Shankland, T., Nitsan, U., Duba, A., 1979. Optical absorption and radiative heat transport in olivine at high temperature. J. Geophys. Res. 84, 1603–1610.
Swanberg, C., 1972. Vertical distribution of heat generation in the Idaho Batholith. J. Geophys. Res. 77, 2508–2513.
Vigneresse, J., Cuney, M., 1991. Are granites representative of heat flow provinces? In: Cermak, V., Rybach, L. (Eds.), Terrestrial Heat Flow and the Lithosphere Structure. Exploration of the Deep Continental Crust. Springer-Verlag, Berlin, Germany, pp. 87–110.
Vitorello, I., Pollack, H., 1980. On the variation of continental heat flow with age and the thermal evolution of the continents. J. Geophys. Res. 85, 983–995.
Walter, M., Katsura, T., Kubo, A., Shinmei, T., Nishikawa, O., Ito, E., Lesher, C., Funakoshi, K., 2002. Spinel–garnet lherzolite transition in the system $CaO–MgO–Al_2O_3–SiO_2$ revisited: an in situ x-ray study. Geochim. Cosmochim. Acta 66, 2109–2121.
Wiechert, U., Ionov, D., Wedepohl, K., 1997. Spinel peridotite xenoliths from the Atsagin-Dush volcano, Dariganga lava plateau, Mongolia: a record of partial melting and cryptic metasomatism in the upper mantle. Contrib. Mineral. Petrol. 126, 345–364.
Xu, X., O'Reilly, S., Griffin, W., Zhou, X., Huang, X., 1998. The nature of the Cenozoic lithosphere at Nushan, eastern China. Mantle Dynamics and Plate Interactions in East Asia. : Geodynamics, 27. Am. Geophys. Union.
Yoshino, T., Matsuzaki, T., Shatskiy, A., Katsura, T., 2009. The effect of water on the electrical conductivity of olivine aggregates and its implications for the electrical structure of the upper mantle. Earth Planet. Sci. Lett. 288, 291–300.
Zheng, J., Griffin, W., O'Reilly, S., Yang, J., Li, T., Zhang, M., Zhang, R., Liou, J., 2006. Mineral chemistry of peridotites from Paleozoic, Mesozoic and Cenozoic lithosphere: constraints on mantle evolution beneath eastern China. J. Petrol. 47, 2233–2256.